Pure Neutron Matter Constraints and Nuclear Symmetry Energy

F J Fattoyev[1,2,*], W G Newton[1,†], Jun Xu[1,‡] and Bao-An Li[1,3,§]

[1]Department of Physics and Astronomy, Texas A&M University-Commerce, Commerce, Texas 75429-3011, USA

[2]Institute of Nuclear Physics, Tashkent 100214, Uzbekistan

[3]Department of Applied Physics, Xian Jiao Tong University, Xian 710049, China

E-mail: *Farrooh.Fattoyev@tamuc.edu, †William.Newton@tamuc.edu, ‡Jun.Xu@tamuc.edu, §Bao-An.Li@tamuc.edu

Abstract. In this review, we will discuss the results of our recent work [1] to study the general optimization of the pure isovector parameters of the popular relativistic mean-field (RMF) and Skyrme-Hartree-Fock (SHF) nuclear energy-density functionals (EDFs), using constraints on the pure neutron matter (PNM) equation of state (EoS) from recent *ab initio* calculations. By using RMF and SHF parameterizations that give equivalent predictions for ground-state properties of doubly magic nuclei and properties of symmetric nuclear matter (SNM) and PNM, we found that such optimization leads to broadly consistent symmetry energy J and its slope parameter L at saturation density within a tight range of $\sigma(J) < 2$ MeV and $\sigma(L) < 6$ MeV. We demonstrate that a clear model dependence shows up (a) in the curvature parameter of the symmetry energy $K_{\rm sym}$, (b) the symmetry energy at supra-saturation densities, and (c) the radius of neutron stars.

1. Introduction

Phenomenological nuclear effective interactions offer a compact description of the *in-medium* nucleon-nucleon interaction and are useful tools in the applications of both the nuclear structure and the astrophysical phenomena. The effective interaction is typically dependent on few parameters representing, for example, coupling constants, which are often fit to well-determined experimental nuclear observables such as binding energies, charge radii, single particle energy spectra and spectra of collective excitations. One of the main objective of modern nuclear many-body theory is to obtain an EDF [2] with clear physical connections to *ab initio* nucleon-nucleon interactions and QCD.

In the recent years, much effort has been devoted to constrain the energy per neutron of PNM ($E_{\rm PNM}$) at sub-saturation densities. By studying the universal behavior of resonant Fermi gases with infinite scattering length, a significant constraint is achieved for the EoS of dilute neutron matter [3]. These calculations have been extended to higher densities using the full power of quantum Monte Carlo methods [4, 5]. Moreover, by studying the physics of chiral three-nucleon forces the EoS of PNM is obtained perturbatively up to nuclear saturation density [6]. Finally, the auxiliary field diffusion Monte Carlo (AFDMC) technique, which takes into account the realistic nuclear Hamiltonian containing modern two- and three-body interactions of the

Argonne potential and Urbana family of three-body nucleon forces, is used to calculate the EoS of PNM up to and above saturation density [7, 8, 9].

In this work we concentrate on the widely used RMF [10, 11] and SHF [12, 13] models, with the latter thought of as a non-relativistic expansion of the former [14, 15]. Both models have less than ten free parameters in their simplest forms. Although there are more than 200 parameter sets in the literature for the SHF model [16] and dozens of parameterizations exist in the simplest form of the RMF model, e.g. [17], many of these sets are old and have been superseded by parameter sets fit to more recent and accurate data. Since the number of experimental observables is usually larger than the number of free parameters, the problem of optimizing these EDFs is generally overdetermined, and this results in a significant degeneracy among parameter sets. Fortunately, one can use the covariance analysis techniques [18, 19] to study correlations between predicted observables from a particular EDF in its model space. We use the linear regression method to optimize the two pure isovector parameters of RMF and SHF models by using the results from the *ab initio* theoretical calculations of the PNM EoS as our 'experimental' constraints. To obtain meaningful theoretical uncertainties for the model parameters, as well as for the predicted observables, we employ the covariance analysis technique. Optimizing the two pure isovector parameters will ensure that the predictions for the well-determined isoscalar observables such as binding energies $B(A)$ and charge radii $R_{\rm ch}$ of doubly magic nuclei will not be affected. We find the best fit values and 1σ confidence intervals on the properties of isospin-asymmetric nuclear matter, such as the symmetry energy parameters. In addition, poorly constrained observables such as the neutron skin thickness of lead and neutron-star radii are predicted from the resulting constraints. We discuss the manifestation of the model dependence in our results, by exploring the symmetry energy at supra-saturation densities and properties of neutron stars. We should note that our aim is not to establish new parameterizations of these EDFs, or to set absolute constraints on symmetry energy, but to explore as far as possible the generic constraints that can be placed by each model on neutron-rich systems once constrained by the information from the PNM EoS.

2. Nuclear Symmetry Energy

The nuclear symmetry energy, $S(\rho)$, is defined as the coefficient of the leading term of isospin asymmetry parameter, $\alpha = (\rho_{\rm n} - \rho_{\rm p})/\rho$, in the expression of the binding energy per nucleon in neutron-rich nuclear matter

$$E(\rho, \alpha) = E_0(\rho) + S(\rho)\alpha^2 + \mathcal{O}(\alpha^4) \ , \tag{1}$$

where ρ is the baryon number density with $\rho_{\rm n}$ ($\rho_{\rm p}$) being the neutron (proton) number density. Around the saturation density ρ_0, one can express the symmetry energy as

$$S(\rho) = J + L\chi + \frac{1}{2}K_{\rm sym}\chi^2 + \mathcal{O}(\chi^3) \ , \tag{2}$$

where $\chi \equiv (\rho - \rho_0)/3\rho_0$, J is the value of the symmetry energy at saturation density, L is the slope parameter, and $K_{\rm sym}$ is the curvature parameter of the symmetry energy at saturation density. The coefficients of the higher-order terms in Eq. (1) are generally much smaller than $S(\rho)$, so it is usually a good approximation to write the symmetry energy as the difference between the energy per nucleon of PNM and SNM, i.e., $S(\rho) \approx E(\rho, 1) - E_0(\rho)$. However, in this work we will not use such an approximation, but rather calculate it from the full analytical expression in a given model.

3. Relativistic Mean-Field and Skyrme-Hartree-Fock Models

We apply the constraints on the microscopic PNM calculations to the two popular phenomenological nuclear many-body models to study the nuclear symmetry energy and related

quantities of nuclear physics and nuclear astrophysics. The commonly used RMF model contains an isodoublet nucleon field (ψ) interacting via the exchange of the scalar-isoscalar σ-meson (ϕ), the vector-isoscalar ω-meson (V^μ), the vector-isovector ρ-meson ($\mathbf{b}^\mu$), and the photon (A^μ) [10, 11, 20]. The effective Lagrangian density for the model can be written as

$$\begin{aligned}\mathcal{L} &= \bar{\psi}\left[\gamma^\mu\left(i\partial_\mu - g_{\rm v}V_\mu - \frac{g_\rho}{2}\boldsymbol{\tau}\cdot\mathbf{b}_\mu - \frac{e}{2}(1+\tau_3)A_\mu\right) - (M - g_{\rm s}\phi)\right]\psi + \frac{1}{2}\partial_\mu\phi\,\partial^\mu\phi - \frac{1}{2}m_{\rm s}^2\phi^2 \\ &- \frac{1}{4}V^{\mu\nu}V_{\mu\nu} + \frac{1}{2}m_{\rm v}^2V^\mu V_\mu - \frac{1}{4}\mathbf{b}^{\mu\nu}\cdot\mathbf{b}_{\mu\nu} + \frac{1}{2}m_\rho^2\,\mathbf{b}^\mu\cdot\mathbf{b}_\mu - \frac{1}{4}F^{\mu\nu}F_{\mu\nu} - U(\phi, V_\mu, \mathbf{b}_\mu)\ , \quad (3)\end{aligned}$$

where $V_{\mu\nu} \equiv \partial_\mu V_\nu - \partial_\nu V_\mu$, $\mathbf{b}_{\mu\nu} \equiv \partial_\mu \mathbf{b}_\nu - \partial_\nu \mathbf{b}_\mu$, and $F_{\mu\nu} \equiv \partial_\mu A_\nu - \partial_\nu A_\mu$ are the isoscalar, isovector, and electromagnetic field tensors, respectively. The nucleon mass M and meson masses $m_{\rm s}$, $m_{\rm v}$, and m_ρ may be treated (if wished) as empirical parameters. The effective potential $U(\phi, V_\mu, \mathbf{b}_\mu)$ consists of non-linear meson interactions that simulates the complicated dynamics encoded in few model parameters. In the present work we use the following form of the effective potential [21]:

$$U(\phi, V^\mu, \mathbf{b}^\mu) = \frac{\kappa}{3!}(g_{\rm s}\phi)^3 + \frac{\lambda}{4!}(g_{\rm s}\phi)^4 - \frac{\zeta}{4!}g_{\rm v}^4(V_\mu V^\mu)^2 - \Lambda_{\rm v}g_\rho^2\,\mathbf{b}_\mu\cdot\mathbf{b}^\mu g_{\rm v}^2 V_\nu V^\nu\ . \quad (4)$$

This model is described by seven interaction parameters: $\{g_{\rm s}, g_{\rm v}, g_\rho, \kappa, \lambda, \zeta, \Lambda_{\rm v}\}$.

The standard form of the energy density obtained from the zero-range Skyrme interaction using the Hartree-Fock method can be written as [22]

$$\begin{aligned}\mathcal{H} &= \frac{\hbar^2}{2M}\tau + t_0\left[(2+x_0)\,\rho^2 - (2x_0+1)\left(\rho_{\rm n}^2 + \rho_{\rm p}^2\right)\right]/4 \\ &+ t_3\rho^\sigma\left[(2+x_3)\,\rho^2 - (2x_3+1)\left(\rho_{\rm n}^2 + \rho_{\rm p}^2\right)\right]/24 \\ &+ \left[t_2\,(2x_2+1) - t_1\,(2x_1+1)\right](\tau_n\rho_n + \tau_p\rho_p)\,/8 + \left[t_1\,(2+x_1) + t_2\,(2+x_2)\right]\tau\rho/8 \\ &+ \left[3t_1\,(2+x_1) - t_2\,(2+x_2)\right](\nabla\rho)^2\,/32 - \left[3t_1\,(2x_1+1) + t_2\,(2x_2+1)\right]\left[(\nabla\rho_{\rm n})^2 + (\nabla\rho_{\rm p})^2\right]/32 \\ &+ W_0\left[\vec{J}\cdot\nabla\rho + \vec{J}_{\rm n}\cdot\nabla\rho_{\rm n} + \vec{J}_{\rm p}\cdot\nabla\rho_{\rm p}\right]/2 + (t_1 - t_2)\left[J_{\rm n}^2 + J_{\rm p}^2\right]/16 - (t_1x_1 + t_2x_2)\,J^2/16\ . \quad (5)\end{aligned}$$

Here ρ_q, τ_q, and $\vec{J}_q$ ($q = {\rm p}, {\rm n}$) are, respectively, the number, kinetic energy, and spin-current densities, and ρ, τ, and $\vec{J}$ are the corresponding total densities. The SHF model is expressed in terms of nine Skyrme parameters: $\{t_0, t_1, t_2, t_3, x_0, x_1, x_2, x_3, \sigma\}$ and the spin-orbit coupling constant W_0, which is taken as 133.3 MeV fm^5 [23] in the present work.

4. Linear Regression and Covariance Analysis Method

The linear regression and covariance analysis method is discussed in details in Ref. [25] and its power has been recently illustrated in Refs. [18, 19, 24]. In a nutshell, one can describe it as follows. First, an optimal parameters set is found for a given phenomenological model $\mathcal{O}_n^{\rm (th)}(\mathbf{p})$ as a function of the F model parameters $\mathbf{p} = (p_1, \ldots, p_F)$, by minimizing the quality measure χ^2 through a method of a least-squares fit:

$$\chi^2(\mathbf{p}) \equiv \sum_{n=1}^{N}\left(\frac{\mathcal{O}_n^{\rm (th)}(\mathbf{p}) - \mathcal{O}_n^{\rm (exp)}}{\Delta\mathcal{O}_n}\right)^2\ , \quad (6)$$

where N is the number of *experimental* observables $\mathcal{O}_n^{\rm (exp)}$ that are determined with an accuracy of $\Delta\mathcal{O}_n$. Then one can compute the symmetric matrix of second derivatives:

$$\chi^2(\mathbf{p}) - \chi^2(\mathbf{p}_0) \equiv \Delta\chi^2(\mathbf{x}) = \mathbf{x}^T\hat{\mathcal{M}}\,\mathbf{x}\ , \quad (7)$$

where $x_i \equiv \frac{(\mathbf{p}-\mathbf{p}_0)_i}{(\mathbf{p}_0)_i}$. The matrix $\hat{\mathcal{M}}$ contains all the information about the behavior of the χ^2 function around the minimum. In particular, one can find the meaningful theoretical uncertainties by computing the statistical covariance of two observables A and B defined as follows:

$$\mathrm{cov}(A,B) = \sum_{i,j=1}^{F} \frac{\partial A}{\partial x_i} (\hat{\mathcal{M}}^{-1})_{ij} \frac{\partial B}{\partial x_j} \,. \tag{8}$$

The variance $\sigma^2(A)$ of a given observable A is then simply given by $\sigma^2(A) = \mathrm{cov}(A,A)$. Finally, one can plot the covariance ellipses between two observables A and B by diagonalizing the 2×2 covariance matrix:

$$\hat{\mathcal{C}} = \begin{pmatrix} \mathrm{cov}(A,A) & \mathrm{cov}(A,B) \\ \mathrm{cov}(B,A) & \mathrm{cov}(B,B) \end{pmatrix} \tag{9}$$

The eigenvalues of this covariance matrix represent the semi-major and semi-minor axes of the covariance ellipse, while the eigenvectors provide the orientation of the ellipse.

For our set of 'experimental' observables $\mathcal{O}_n^{(\mathrm{exp})}$ in the χ^2 input we choose the theoretical microscopic calculations of the energy per neutron E_{PNM} in the density range of $0.04 \leq \rho \leq 0.16$ fm^{-3} [6, 7, 26]. We restrict our experimental input to this band only, where the upper bound is the PNM results at saturation density, as the extension of the PNM calculations to higher densities using piecewise polytropes in the chiral effective theory [27] was shown to allow a huge uncertainty window in the EoS. Moreover, the symmetry energy coefficients should only be sensitive to the EoS around the saturation density.

5. Results

We first identify that the two parameters in each model—g_ρ and Λ_{v} in the RMF model [28], and x_0 and x_3 in the SHF model—are *solely* isovector parameters. The change of these parameters affects only the isovector sensitive properties of nuclear matter, such as the symmetry energy $S(\rho)$, while the EoS of SNM and therefore properties of SNM, such as saturation density ρ_0, binding energy per nucleon at saturation density E_0, incompressibility coefficient at saturation density K_0, and isoscalar effective mass M^* at saturation all remain unchanged. Therefore we optimize these two isovector parameters [$F = 2$ in Eqs. (7) and (8)] with respect to the available range of PNM equations of state to constrain the values of the symmetry energy parameters at saturation density by using the linear regression and covariance analysis method discussed in the previous section. Note that most properties of the SNM are constrained experimentally within less than 10%. However, the EoS of PNM predicted by various parameterizations of both models differ significantly. Although some of them fall within the band of the microscopic PNM calculations, for most of the parameterizations there is almost no or very little agreement with these calculations as can be seen from Fig. 1 (a). Therefore, in general, the RMF and the SHF model predictions for the symmetry energy parameters are substantially different. Once the two isovector parameters are optimized to the energy per neutron E_{PNM} predictions at sub-saturation densities [See Fig. 1 (b)], we find that the symmetry energy parameters at saturation can also be significantly constrained (See Table 1).

To further assess theoretical uncertainties in the symmetry energy parameters, we select the accurately-calibrated NL3* [29] and the recent IU-FSU [30] parametrizations from the RMF model. The IU-FSU is the recent parametrization that predicts a very soft symmetry energy, and was validated against experimental, observational, and theoretical data, while the accurately-calibrated NL3* parametrization gives a much stiffer EoS of both SNM (larger value of K_0 and smaller value of ζ parameter) and a stiff symmetry energy (larger values of symmetry energy J and slope L) and therefore offers a suitable contrast to IU-FSU.

To compare the RMF and SHF models on the same basis, we create two SHF parametrizations which give the same properties of nuclear matter at saturation as the two RMF parametrizations

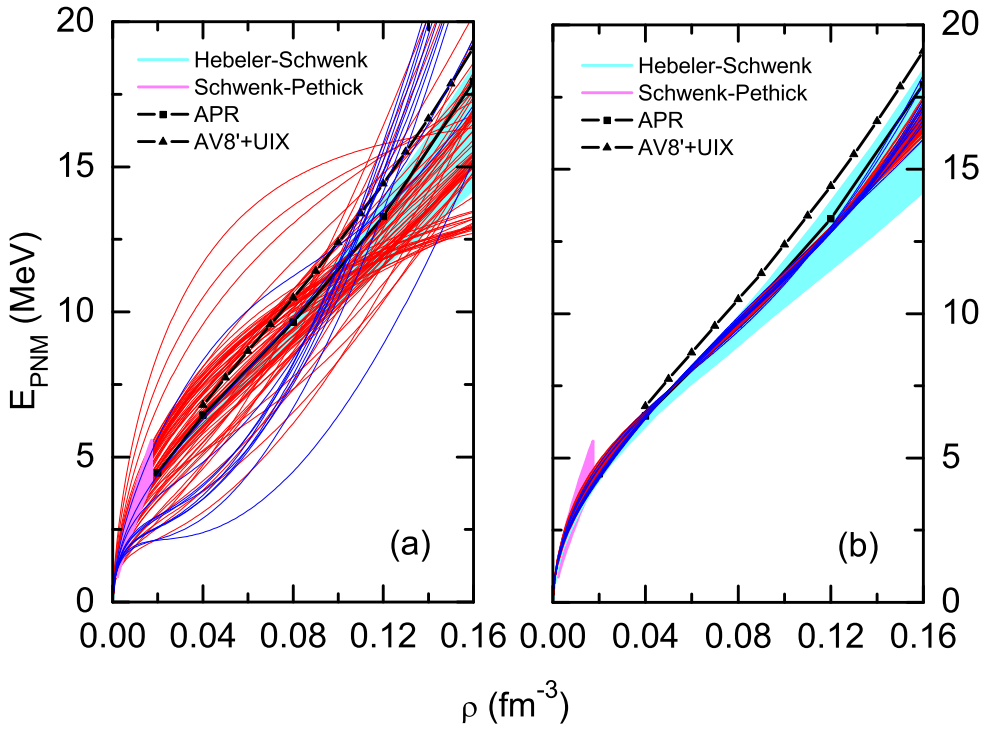

Figure 1. Comparing the PNM EoS from 11 RMF (blue lines) and 73 SHF parameterizations (red lines) that are produced since 1995, with the AFDMC EoS in the AV8′+UIX Hamiltonian [9], the variational APR EoS [26], the low-density band from the constraints of resonant Fermi gases [3], and the high-density band from the chiral effective field theory calculations with 3-neutron forces [6], before (a) and after (b) the PNM optimization.

Table 1. Predicted ranges for symmetry energy parameters within RMF and SHF models before (with superscript '0') and after (without superscript '0') their pure isovector parameters optimized to PNM, and taking into account all remaining variation from parameterizations constructed since 1995.

	J^0 (MeV)	J (MeV)	L^0 (MeV)	L (MeV)	K_τ^0 (MeV)	K_τ (MeV)
RMF	30.3 – 38.7	30.2 – 31.4	47.2 – 122.7	36.1 – 59.3	-701.7 – -195.3	-329.7 – -215.7
SHF	27.8 – 39.6	30.1 – 33.2	5.8 – 100.1	28.5 – 64.4	-514.8 – -266.3	-418.8 – -235.3

(See Table 2), through the method of writing the Skyrme parameters as functions of macroscopic nuclear quantities [23, 31]. These new parametrizations are referred to as SkNL3* and SkIU-FSU forces [1].

Several definitions of the nucleon effective mass exist in the literature [32]. In the RMF model the Dirac effective mass is defined through the scalar part of the nucleon self-energy in the Dirac equation. It has been well documented that there is a strong correlation between the Dirac effective nucleon mass at saturation density $M_{\rm D}^*$ and the strength of the spin-orbit force in nuclei [11, 14, 33, 34]. Indeed, one of the most compelling features of RMF models is the

Table 2. Macroscopic quantities from four reference parameterizations. They are the nuclear saturation density ρ_0, the binding energy per nucleon E_0 and incompressibility K_0 of SNM at saturation, the symmetry energy J and its slope parameter L at saturation, and the nucleon effective mass M^* at saturation. For consistency, we present the Lorentz effective mass of the RMF model, which is set equal to the isovector and isoscalar effective masses in the SHF model.

	ρ_0 (fm^{-3})	E_0 (MeV)	K_0 (MeV)	J (MeV)	L (MeV)	M^* (M)
NL3*	0.1500	−16.32	258.49	38.7	122.7	0.671
SkNL3*	0.1527	−15.76	258.49	38.7	122.7	0.671
IU-FSU	0.1546	−16.40	231.33	31.3	47.2	0.687
SkIU-FSU	0.1575	−15.70	231.33	31.3	47.2	0.687

reproduction of the spin-orbit splittings in finite nuclei. It is shown that models with effective masses outside the range $0.58 < M^*_{\rm D}/M < 0.64$ will not be able to reproduce empirical spin-orbit couplings [35], when no tensor couplings are taken into account. On the other hand, the non-relativistic effective mass parameterizes the momentum dependence of the single particle potential, which is the result of a quadratic parametrization of the single particle spectrum. A recent study [16] puts a bound of $0.69 < M^*/M < 1.0$ for the non-relativistic effective masses. It has been argued [36] that the so-called Lorentz mass $M^*_{\rm L}$ should be compared with the non-relativistic effective mass extracted from analyses carried out in the framework of nonrelativistic optical and shell models. For consistency, we choose the effective mass in the SHF parameterizations to be equal to the Lorenz mass in the RMF parameterizations (See the last column of Table 2). Since the RMF model we use in this work gives the same isoscalar and isovector effective masses, we set them equal in the reference SHF model too. Finally, the isoscalar parameters of the two reference Skyrme forces are then re-adjusted to fit the binding energy and charge radius of ^{208}Pb by adjusting only the saturation density ρ_0 and the binding energy E_0 of SNM. These ensure that the predictions for the charge radii and binding energies of other doubly closed-shell nuclides will be within 1-2% accuracy. In terms of the predicted values of isoscalar and isovector bulk observables, both corresponding RMF and SHF models are therefore almost equivalent.

Having obtained the PNM optimized parameter sets, the 1σ errors on these two purely isovector parameters can be translated into equivalent errors on the symmetry energy parameters and the neutron skin thickness of ^{208}Pb using the covariance analysis (See Table 3). The errors in J are less than ± 1 MeV for all the parameterizations. The RMF model gives a relatively small error in L of around ± 2 MeV, while the SHF model gives a much larger error around ± 6 MeV. Table 3 appears to indicate that within the 1σ errors, both models are consistent in their predicted values of J and L. However, a 1σ joint confidence regions in the J-L plane plotted in Fig. 2(a) for both RMF and SHF models shows that in fact the two models predict non-overlapping regions in J-L space. Both models show a positive correlation between J and L, but with differing slopes. The origin of this difference lies mainly in the values of the higher-order symmetry energy parameters that are predicted upon optimization. There is a strong model dependency in the prediction for the curvature parameter of the symmetry energy $K_{\rm sym}$ (see Table 3). For example, after the PNM optimization IU-FSU predicts $K_{\rm sym} = -6.8 \pm 12.9$ MeV, while its Skyrme-like version predicts a smaller value of $K_{\rm sym} = -130.2 \pm 13.3$ MeV. When we plot the 1σ joint confidence regions in the $K_{\rm sym}$-L plane for both RMF and SHF models [see Fig. 2 (b)] further differences can be seen: there is, generically, a negative correlation between the slope of the symmetry energy and $K_{\rm sym}$ in the RMF model, while this correlation is positive in the case of the SHF model.

Table 3. Isovector observables and associated 1σ error bars from four reference parameterizations after the PNM constraints are applied. Values are shown for the symmetry energy at $\rho = 0.1$ fm^{-3} $S_{0.1}$ and at saturation density J, slope parameter L, curvature parameter $K_{\rm sym}$, isospin-dependent part of incompressibility K_τ, and the neutron skin thickness $R_{\rm skin}$ of ^{208}Pb. All the quantities are in MeV apart from $R_{\rm skin}$, which is in fm.

	$S_{0.1}$	J	L	$K_{\rm sym}$	K_τ	$R_{\rm skin}$
NL3*	24.9 ± 0.4	30.7 ± 0.7	50.3 ± 1.8	39.2 ± 17.8	-284.6 ± 29.4	0.18 ± 0.01
SkNL3*	24.5 ± 0.3	31.0 ± 0.9	46.4 ± 6.4	62.7 ± 16.6	-380.0 ± 15.2	0.16 ± 0.01
IU-FSU	24.9 ± 0.4	31.4 ± 0.7	52.9 ± 2.0	-6.8 ± 12.9	-257.6 ± 22.3	0.18 ± 0.01
SkIU-FSU	24.4 ± 0.3	31.4 ± 0.9	48.0 ± 6.2	-130.2 ± 13.3	-343.9 ± 15.3	0.16 ± 0.01

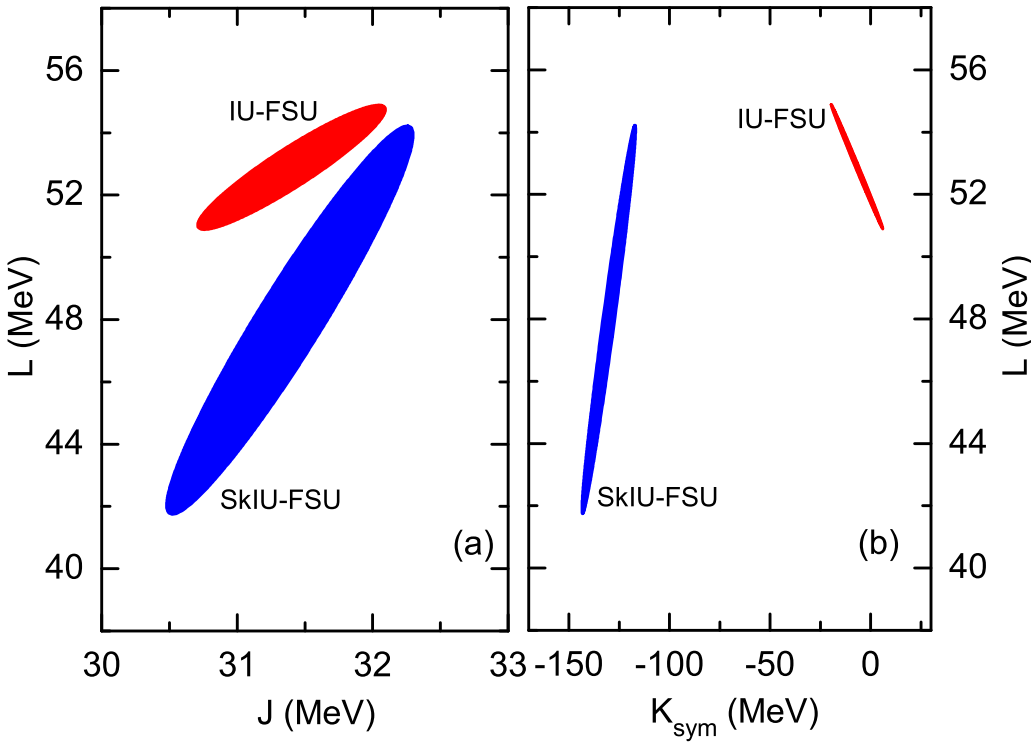

Figure 2. 1σ joint confidence regions for the symmetry energy J and its slope parameter L (a), and for the slope parameter L and curvature parameter $K_{\rm sym}$ (b) of the symmetry energy at saturation density from the IU-FSU and SkIU-FSU parameterizations.

Particularly attractive are predictions for the neutron skin thickness of ^{208}Pb after the PNM optimization. The original NL3* parametrization predicts a very thick neutron skin of $R_{\rm skin} = 0.29$ fm, while its Skyrme counterpart predicts a value of $R_{\rm skin} = 0.27$ fm. On the other hand, both the original IU-FSU and SkIU-FSU parameterizations predict a much lower value of $R_{\rm skin} = 0.16$ fm for ^{208}Pb. These values are consistent with the current experimental result of $R_{\rm skin} = 0.33^{+0.16}_{-0.18}$ fm for the neutron skin thickness of lead obtained using electroweak probes in the PREX experiment [37]. After the PNM optimization, we find that in general the RMF model

predicts $R_{\rm skin} = 0.18 \pm 0.01$ fm for ^{208}Pb, while the SHF model predicts $R_{\rm skin} = 0.16 \pm 0.01$ fm (See Table 3), which are marginally consistent with each other within the 1σ error-bars. Thus both models generically predict a thin neutron skin thickness of lead. Moreover, the error-bars coming from this constraint are very small. This is a particularly provocative result, since if the new PREX experiment reduces the error bars without moving the central value for the neutron skin, almost all current models of the nuclear structure would need to be modified. Also, this would appear to call for a significant modification of the PNM microscopic calculations.

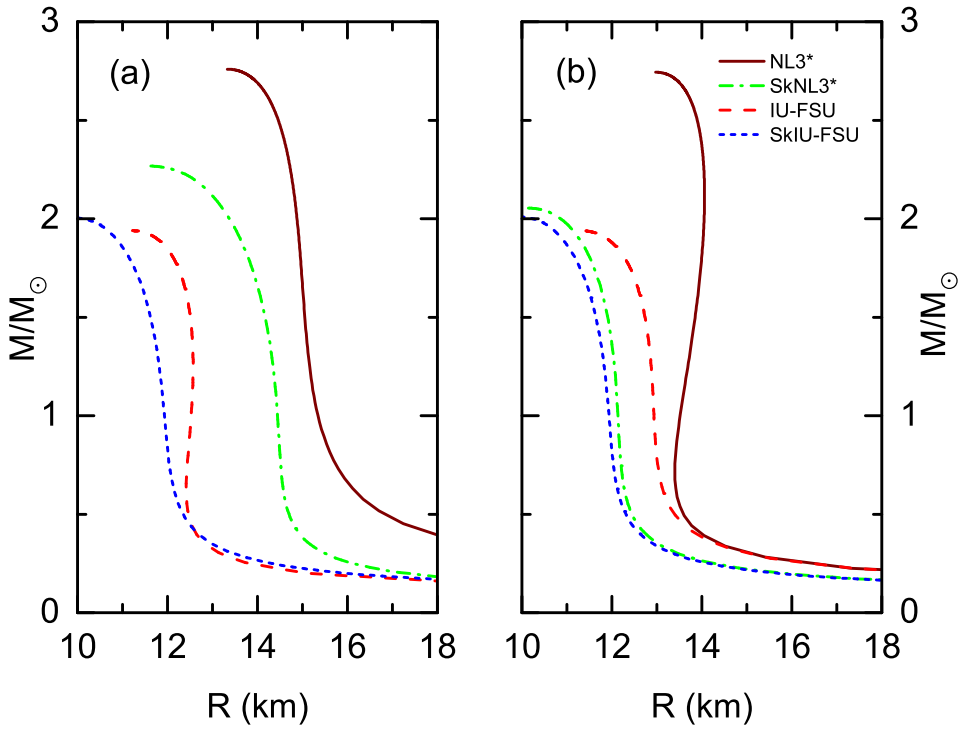

Figure 3. Mass-vs-radius relation of neutron stars calculated from the four parameterizations before (a) and after (b) the PNM optimization (Figure is taken from Ref. [1]).

Finally, we apply our results to the neutron star structure, by extrapolating the EoS from the RMF and the SHF models to higher densities. The neutron star matter is assumed to be charge neutral and in the β-equilibrium condition with neutrons, protons, electrons, and muons. No exotic degrees of freedom are assumed. The equations of state from the four parametrization are then utilized in the general relativistic equation of stellar structure (known as the Tolman-Oppenheimer-Volkoff equation) to obtain the mass-*vs*-radius relation. In Fig. 3 (a) we display mass-*vs*-radius relations as predicted by the four original RMF and SHF parametrizations that predict a wide range of results for low mass neutron star radii. This can be mainly attributed to the density dependence of the symmetry energy, which is quite different in the original two parameterizations. Once calibrated to the PNM results, this difference almost vanishes within the same model as shown in the Fig. 3 (b), i.e., both RMF and SHF parameterizations now match each other more closely. The only difference at high masses between the RMF parametrizations is now due to the ζ parameter that results in a stiffer EoS of SNM in NL3* parameterizations at several times saturation density. Although both NL3* and IU-FSU parameterizations in a given RMF or SHF model predict similar radii, there is a clear difference between the RMF and

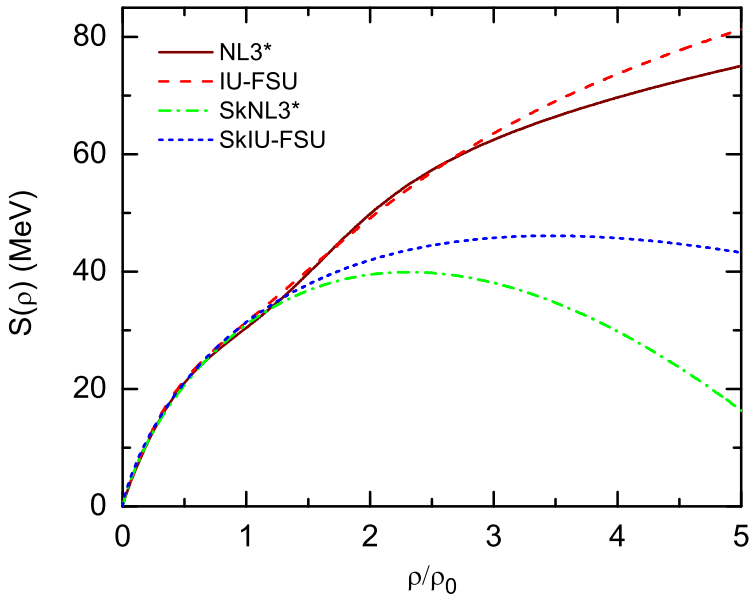

Figure 4. Density dependence of symmetry energy from the four parameterizations after the PNM optimization (Figure is taken from Ref. [1]).

the SHF predictions as a whole. In the case of IU-FSU and SkIU-FSU we have almost a ~ 1 km difference for the radius of a canonical neutron star. This discrepancy is even larger in the case of NL3*, which is about ~ 1.8 km. Thus, there is a strong model dependence when the two models are applied to neutron star structure calculations after the same PNM optimization. This model dependence primarily comes from the different density dependence of symmetry energy at supra-saturation densities. Looking at Fig. 4 we see that the symmetry energy is almost the same in all the models up to $\sim 1.5\rho_0$. The RMF model predicts a monotonic increasing function of density for the symmetry energy, while the SHF model tends to give a decreasing symmetry energy at higher densities. We thus show that the low-density PNM constraints alone result in a distinct model dependency of radius predictions. With the similar saturation properties of nuclear matter constrained by the PNM EoS, one can obtain different radii for a given neutron star mass. Although the PNM optimization tightly constrains the symmetry energy up to a little above the saturation density, its high density behavior that is very crucial in determining neutron star radii, still remain unclear. To elucidate this long-standing problem further we need to rely on the heavy-ion collision experiments [38, 39, 40] and neutron star observations [41, 42].

6. Summary

Using our best knowledge of the PNM EoS below and around saturation density from *ab initio* calculations, we constrain the density dependence of the symmetry energy for the RMF and SHF models, by optimizing the two pure isovector parameters from each model while keeping the values of other parameters so that the errors of predicted binding energies and charge radii of medium to heavy nuclei remain to be less than 2%.

We show that such fits result in very similar predictions for the symmetry energy J and its slope parameter L at saturation density from both models as long as the nucleon effective mass from both RMF and SHF models is chosen to be consistent [36, 35]. When the error bounds

are plotted as ellipses in the J-L plane, a positively-correlated relationship between J and L is observed for both models. However, different slopes are obtained from the RMF and SHF models, and the two ellipses have no overlapping area in the plane. This model dependence comes from the different values of $K_{\rm sym}$ and higher-order symmetry energy parameters.

Predictions of a neutron skin thickness $R_{\rm skin}$ for ^{208}Pb are similar from both models and are within the error-bar of the latest experimental data. Both models predict a very thin neutron skin. Although the PNM constraints lead to broadly similar behaviors of the symmetry energy as a function of density up to $\approx 1.5\rho_0$, they deviate significantly at higher densities due to the differences in the functional form of the symmetry energy. This results in a striking difference in the predictions of the neutron star radii from both models.

We showed the possible differences in predictions from two phenomenological energy-density functional forms, when the same experimental or theoretical constraints up to saturation density are applied. Care must be taken interpreting observational and experimental constraints from different nuclear models, and searching for a robust and better-determined EDF is necessary.

7. Acknowledgments

This work is supported in part by the National Aeronautics and Space Administration under grant NNX11AC41G issued through the Science Mission Directorate, and the National Science Foundation under Grants No. PHY-1068022 and No. PHY-0757839.

8. References

[1] Fattoyev F J, Newton W G, Xu J and Li B -A 2012 *Phys. Rev. C* **86** 025804
[2] *Building a universal nuclear energy density functional* (UNEDF Collaboration) http://unedf.org
[3] Schwenk A and Pethick C J 2005 *Phys. Rev. Lett.* **95** 160401
[4] Gezerlis A and Carlson J 2010 *Phys. Rev. C* **81** 025803
[5] Gezerlis A and Carlson J 2011 *Preprint* 1109.4946
[6] Hebeler K and Schwenk A 2010 *Phys. Rev. C* **82** 014314
[7] Gandolfi S, Illarionov A Yu, Schmidt K E, Pederiva F and Fantoni S 2009 *Phys. Rev. C* **79** 054005
[8] Gandolfi S, Illarionov A Yu, Fantoni S, Miller J C, Pederiva F and Schmidt K 2010 *Mon. Not. Roy. Astron. Soc.* **404** L35
[9] Gandolfi S, Carlson J and Reddy S 2012 *Phys. Rev. C* **85** 032801
[10] Serot B D and Walecka J D 1986 *Adv. Nucl. Phys.* **16** 1
[11] Serot B D and Walecka J D 1997 *Int. J. Mod. Phys. E* **6** 515
[12] Skyrme T H R 1956 *Phil. Mag.* **1** 1043
[13] Vautherin D and Brink D M 1972 *Phys. Rev. C* **5** 626
[14] Reinhard P -G 1989 *Rept. Prog. Phys.* **52** 439
[15] Sulaksono A, Burvenich T, Maruhn J A, Reinhard P -G and Greiner W 2003 *Annals Phys.* **308** 354
[16] Dutra M, Lourenço O, Martins J S, Delfino A Stone J R and Stevenson P D 2012 *Phys. Rev. C* **85** 035201
[17] Chen L -W, Ko C M and Li B -A 2007 *Phys. Rev. C* **76** 054316
[18] Reinhard P -G and Nazarewicz W 2010 *Phys. Rev. C* **81** 051303
[19] Fattoyev F J and Piekarewicz J 2011 *Phys. Rev. C* **84** 064302
[20] Mueller H and Serot B D 1996 *Nucl. Phys. A* **606** 508
[21] Todd-Rutel B G and Piekarewicz J 2005 *Phys. Rev. Lett.* **95** 122501
[22] Chabanat E, Meyer J, Bonche P, Schaeffer R and Haensel P 1997 *Nucl. Phys. A* **627** 710
[23] Chen L -W, Ko C M and Li B -A 2010 *Phys. Rev. C* **82** 024321
[24] Fattoyev F J and Piekarewicz J 2012 *Phys. Rev. C* **86** 015802
[25] Brandt S 1999 *Data Analysis: Statistical and Computational Methods for Scientists and Engineers*, 3rd Ed (New York: Springer)
[26] Akmal A, Pandharipande V R and Ravenhall D G 1998 *Phys. Rev. C* **58** 1804
[27] Hebeler K, Lattimer J M, Pethick C J and Schwenk A 2010 *Phys. Rev. Lett.* **105** 161102
[28] Horowitz C J and Piekarewicz J 2001 *Phys. Rev. Lett.* **86** 5647
[29] Lalazissis G A, Karatzikos S, Fossion R, Pena-Arteaga D, Afanasjev A V and Ring P 2009 *Phys. Lett. B* **671** 36
[30] Fattoyev F J, Horowitz C J, Piekarewicz J and Shen G 2010 *Phys. Rev. C* **82** 055803
[31] Chen L -W, Cai B -J, Ko C M, Li B -A and Xu J 2009 *Phys. Rev. C* **80** 014322

[32] van Dalen E N E, Fuchs C and Faessler A 2005 *Phys. Rev. Lett.* **95** 022302
[33] Gambhir Y, Ring P and Thimet A 1990 *Annals Phys.* **198** 132
[34] Bodmer A 1991 *Nucl. Phys. A* **526** 703
[35] Furnstahl R J, Rusnak J J and Serot B D 1998 *Nucl. Phys. A* **632** 607
[36] Jaminon M and Mahaux C 1989 *Phys. Rev. C* **40** 354
[37] Abrahamya et al. 2012 *Phys. Rev. lett.* **108** 112502
[38] Danieleweicz P, Lacey R and Lynch W G 2002 *Science* **298** 1592
[39] Li B -A, Chen L -W and Ko C M 2008 *Phys. Rept.* **464** 113
[40] Baran V, Colonna M, Greco V and Di Toro M 2005 *Phys. Rept.* **410** 335
[41] Lattimer J M and Prakash M 2007 *Phys. Rept.* **442** 109
[42] Steiner A W, Prakash M, Lattimer J M and Ellis P J 2005 *Phys. Rept.* **411** 325